P7.2

# A VARIATIONAL, PSEUDO-MULTIPLE DOPPLER RADAR ANALYSIS TECHNIQUE FOR MOBILE, GROUND-BASED RADARS


Christopher C. Weiss
Texas Tech University, Lubbock, Texas

Howard B. Bluestein
University of Oklahoma, Norman, Oklahoma

Andrew Pazmany
ProSensing, Inc., Amherst, Massachusetts


## 1. INTRODUCTION

The primary tool of research used in the study of many atmospheric phenomena, including drylines, is Doppler radar, owing to its ability to sense remotely radial wind velocity over a large region of space in a short period of time. However, the processing of Doppler data is non-trivial, limited by the designs of both the instrument and the collection method.

Doppler radars provide the radial component of motion along the line of sight of the radar beam only. Therefore, no information on the wind component normal to the line of sight is available. However, for multiple radar systems that observe a region of space simultaneously (at some distance apart, from different viewing angles), it is possible over a limited domain to calculate wind components in non-radial planes. This process is often referred to as *dual-Doppler synthesis* or in general for more than one radar, *multiple-Doppler synthesis*. These techniques can generally be classified as either traditional or variational (or a hybrid of both). Traditional techniques are generally iterative, and involve iterations between diagnostic equations for the dependent variables. Therefore, the unknown analysis variables are found in a non-simultaneous manner. Variational techniques incorporate all dependent analysis variables into one minimized functional, and these variables are usually solved simultaneously.

The primary goal of this study was to develop a variational processing technique for mobile ground-based radar data.

## 2. SCANNING STRATEGY

Range-height indicators (RHIs) are commonly used to sense the vertical structure of atmospheric phenomena (e.g., Parsons et al. 1991) (FIG 1a). Traditionally, RHIs have been performed with a stationary platform. While the fixed platform allows for direct detection of temporal changes in reflectivity and radial velocity, it is very difficult – if not impossible – to retrieve accurately the individual horizontal and vertical components of motion (e.g., the *u* and *w* wind components for an east-west RHI).

However, if the platform is allowed to travel during RHI collection (a strategy hereafter referred to as a rolling RHI (RRHI) (FIG. 1b)), reasonably accurate horizontal and vertical wind components can be synthesized from the time series of radial velocity data. The remainder of the paper highlights the development and testing of a procedure that utilizes RRHI data collection in such a manner.

## 3. DEVELOPMENT OF THE VARIATIONAL TECHNIQUE

A weak-constrant variational (Sasaki 1970) wind synthesis technique was developed for rolling RHI data taken in an east-west plane. The cost function to be minimized was:

$$J = J_{obs} + \beta J_{continuity} \tag{1a}$$

$$J_{obs} = \sum_{n=1}^{m(x,z)} \left( c_1^n u + c_2^n w - V_r^n \right)^2 \tag{1b}$$

$$J_{continuity} = \left( \partial u / \partial x + \partial w / \partial z + \kappa w \right)^2 \tag{1c}$$

$$c_1 = \cos(\alpha) \tag{1d}$$

$$c_2 = \sin(\alpha) \tag{1e}$$

where (1b) represented the contribution to the cost function from observational discrepancy and (1c) denoted the contribution to the cost function from anelastic mass continuity violation. In equations

(1a) - (1e) $u$ and $w$ were the analysis values, $V_r$ was the observed radial velocity, $c_1$ and $c_2$ represented geometric coefficients mapping velocities from Cartesian space to that of the radial velocity vectors, $\kappa$ was the correction to mass continuity for vertical density stratification (assumed constant here), $m$ was the total number of observations per gridpoint of which $n$ was a specific observation, and $\alpha$ was the elevation angle for each observation. The formulation was similar to that developed by Gao et. al (1999) (less a background and smoothness constraint) and Dowell and Bluestein (2002) (neglecting variations in the $y$ direction).

The variations of $J$ with respect to $u$ and $w$ were set equal to zero, yielding two coupled Euler-Lagrange equations (not shown). The two equations were repeatedly solved in turn until the solutions for $u$ and $w$ over the entire domain converged.

## 4. TESTING

To test the analysis technique developed above, a series of observational system simulation experiments (OSSEs) were developed. For each OSSE, model output was sampled by a “pseudo-radar” in a manner similar to that of a typical RRHI data collection. The result of this operation was a time series of radial velocity data, which was then used in conjunction with the variational analysis technique. Since the “truth” was already known (i.e., the model state from which the radial velocity was sampled), exact error statistics could be generated. These statistics revealed the accuracy of the synthesis techniques and allowed for the determination of optimal scanning strategies.

The first OSSE developed was an analytical constant horizontal flow field of 10 m $s^{-1}$ (i.e., $u$=10 m $s^{-1}$) over the entire domain. This flow was sampled using a rolling RHI technique, using a constant platform velocity of 30 mph (13.33 m $s^{-1}$) and vertical antenna rotation rate (hereafter scan rate) of 1.6 degrees $s^{-1}$. The beamwidth of the radar was 0.18 degrees, consistent with the design of the W-band mobile radar from the University of Massachusetts (UMass) (Bluestein and Pazmany 2000). Data were “processed” at 10 Hz. A first guess of u=w=0 was introduced as a first guess to the variational synthesis procedure.

The results from this experiment (FIG. 2) show that the technique was successful at reproducing the horizontal flow with very little error. The RMS error for the domain was calculated to be 0.28 m $s^{-1}$.

Multiple simulations were performed to test the sensitivity of the analysis RMS error to the scanning strategy of the hypothetical radar. The first series of experiments varied the platform velocity from 0.44 m $s^{-1}$ to 31.11 m $s^{-1}$ while holding the scan rate fixed at 2.0 degrees $s^{-1}$. The resulting plot of RMS error (FIG. 3) showed clearly an increase in RMS error as the platform velocity was increased (e.g., RMS = 0.014 m $s^{-1}$ for a platform velocity of 4.44 m $s^{-1}$, and RMS = 0.416 m $s^{-1}$ for a platform velocity of 20.00 m $s^{-1}$). The increase in RMS error was attributed largely to sub-critical look angle differences over portions of the domain. The analysis of $u$ for the high-RMS case (with platform velocity of 20.00 m $s^{-1}$) (FIG. 4a) showed the largest error near the top of the domain, where look angle differences were in the range of zero to 10 degrees (e.g., Fig. 4b). In these sub-critical regions, the radial velocity observations were nearly collinear. Therefore, the retrieval of the individual components of motion ($u$/$w$) was less accurate.

A similar increase in RMS error was seen for a decrease in scan rate with the platform velocity held constant at 13.33 m $s^{-1}$ (FIG. 5). Again, the error increase was correlated with the presence of sub-critical look angle differences.

It was desirable to test how the technique performed in regions with strong gradients in wind direction and velocity, similar to the environment near atmospheric boundaries. To this end, an OSSE was developed using output from a Large Eddy Simulation (LES) (Fedorovich and Conzemius, 2003, personal communication). The LES was designed to simulate the structure of a highly-sheared, strongly-heated convective boundary layer.

A plan view of $w$ at 900 m AGL (FIG. 6) shows clearly a southwest-to-northeast-oriented axis of convergence and upward motion in the center of the domain, associated with a horizontal convective roll.

An east-west vertical cross section was plotted across the LES domain to show the vertical structure of the HCR (FIG. 7a). Upward motion in the HCR extended to approximately 1.5 km AGL, and was about 1 km wide. Weaker regions of generally subsiding air extended over the remainder of the domain. The model output was sampled by the UMass pseudo-radar. The radar platform was assumed to be moving westward with a velocity of 13.33 m $s^{-1}$ and a scan rate of 1.5 degrees $s^{-1}$.

When measured against the actual LES output (the “truth”), an RMS error of 0.568 m $s^{-1}$ was calculated. The analysis qualitatively reproduced all of the features, even those very small in scale. Most of the RMS error accrued in the upper portion of the domain, near and above 2 km AGL. As demonstrated in the constant-flow case above, this region had sub-critical look angle differences, and therefore collinearity amongst the radial velocity observations.

To this point, it was assumed that the UMass pseudo-radar was a perfect instrument. In other words, the data were assumed to contain no observational error. In reality, observational error is present in all measurement platforms. Sources of error include: instrument noise (from the receiver), representativeness (e.g., beam spreading, ducting) and others. To simulate the effect of the instrument error, a Gaussian (i.e., random normal) error was added to the observations.

As expected, the magnitude of the RMS error was higher than the perfect-observation control run, but still small in comparison to the wind velocity. A comparison of the OSSE output with the LES output ("truth") for the control platform velocity of 13.33 m $s^{-1}$, scan rate of 1.6 deg $s^{-1}$ and observational error standard deviations of 1.0 m $s^{-1}$ and 2.0 m $s^{-1}$ (Fig. 8) showed that the variational analysis technique did a very good job at reproducing all of the features in the domain (RMS error = 0.751 m $s^{-1}$ and 1.093 m $s^{-1}$ for error standard deviations of 1.0 m $s^{-1}$ and 2.0 m $s^{-1}$, respectively). As before, performance was worst in the upper portion of the analysis domain where radar coverage was not sufficient.

## 5. APPLICATION

On 22 May 2002, in association with the International $H_2O$ Project, the mobile W-band radar from the UMass collected RRHI data for a dryline in the Oklahoma panhandle. The variational technique developed above was applied successfully to these data. The reader is referred to paper 16A.6 for a report of these results.

## 6. SUMMARY

A new, ground-based, pseudo-multiple Doppler processing technique was developed to analyze rolling RHI data. The technique used variational calculus to find an "optimal" analysis that satisfied radial velocity observations and anelastic mass continuity in a least squares sense. Testing of this technique demonstrated its robustness, even for flows containing a large amount of variability (e.g., an LES). The procedure, as expected, demonstrated its worst results for situations in which radial velocities were collinear. The accuracy of the retrieval depended on both the platform motion and scan rate. Both of these parameters must be considered in determining the optimal scan strategy.

Much potential exists for the wind synthesis technique, and more testing is planned for the future.

## 6. ACKNOWLEDGMENTS

This work was supported by National Science Foundation (NSF) grants ATM-9912097 and ATM-0241037. Thanks to David Dowell and Alan Shapiro for their useful insight into variational radar data processing. Ming Xue assisted in the use of ZXPLOT. Brendan Fennell drove the UMass vehicle for the 22 May 2002 data collection.

## 7. REFERENCES

Bluestein H. B., and A. L. Pazmany, 2000: Observations of tornadoes and other convective phenomena with a mobile, 3–mm wavelength, Doppler radar: The spring 1999 field experiment**.** *Bull. Amer. Meteor. Soc.*, **81**, 2939–2952.

Dowell, D. C., and H. B. Bluestein, 2002: The 8 June 1995 McLean, Texas, Storm. Part I: Observations of cyclic tornadogenesis. *Mon. Wea. Rev.*, **130**, 2626-2648.

Gao, J., M. Xue, A. Shapiro, and K. K. Droegemeier, 1999: A variational method for the analysis of three-dimensional wind fields from two Doppler radars. *Mon. Wea. Rev.,* **127**, 2128-2142.

Parsons, D. B., M. A. Shapiro, R. M. Hardesty, R. J. Zamora, and J. M. Intrieri, 1991: The finescale structure of a west Texas dryline. *Mon. Wea. Rev.*, **119**, 1283-1292.

Sasaki, Y., 1970: Some basic formalisms in numerical variational analysis. *Mon. Wea. Rev.*, **98**, 875-883.

a)

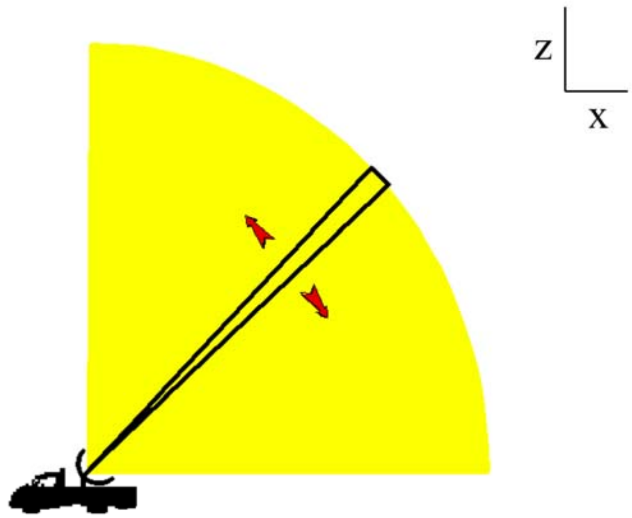


FIG. 1. a) Schematic of SRHI mode of data collection

b)

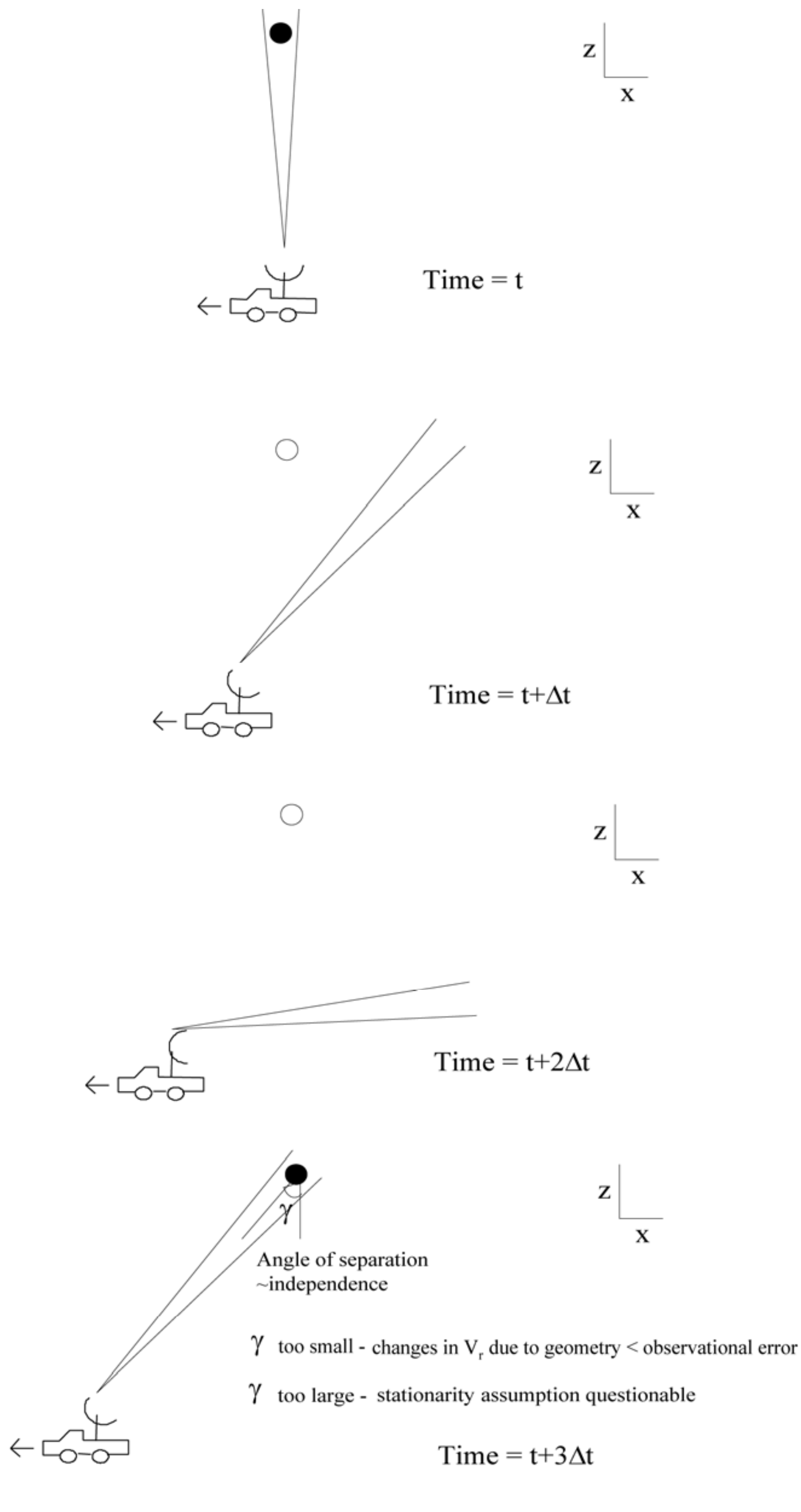


FIG. 1 (cont'd). b) Schematic of RRHI method of data collection.

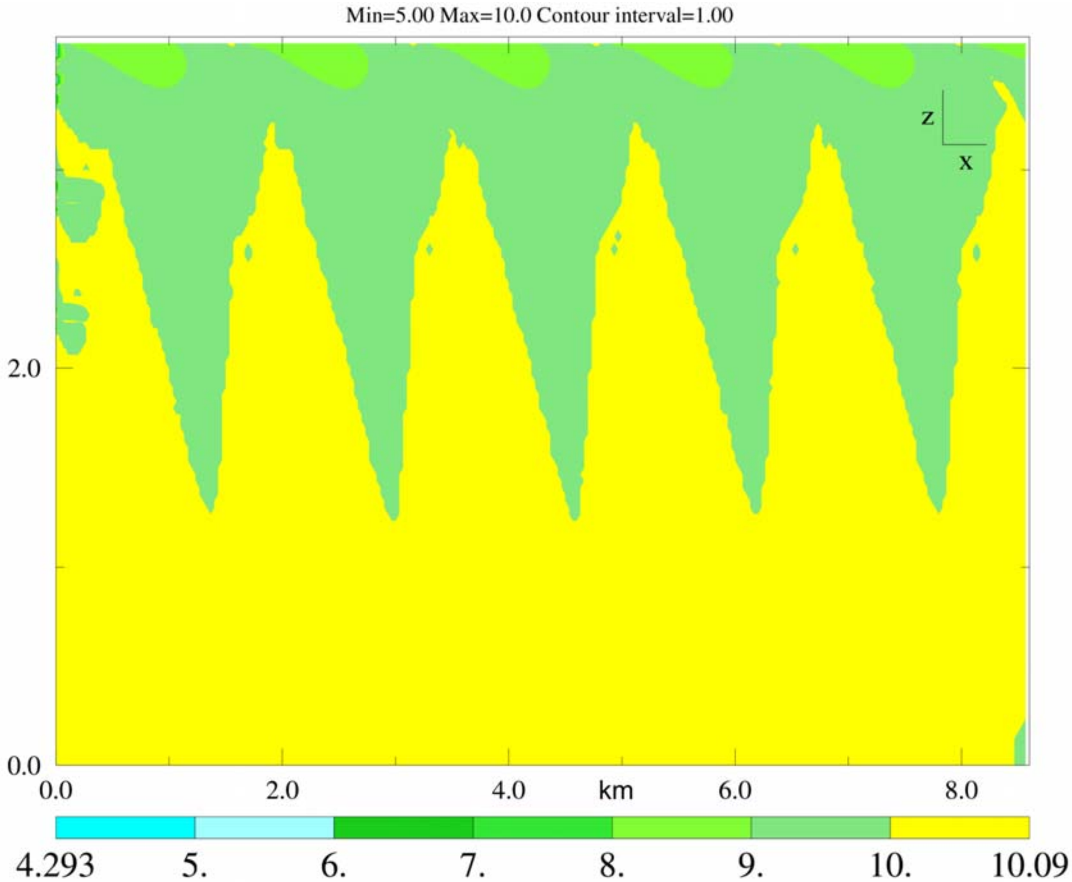


FIG. 2. Analysis *u*-component wind (m $s^{-1}$) for the constant flow (u=10 m $s^{-1}$) OSSE with a truck velocity of 13.33 m $s^{-1}$ and scan rate of 1.6 deg $s^{-1}$.

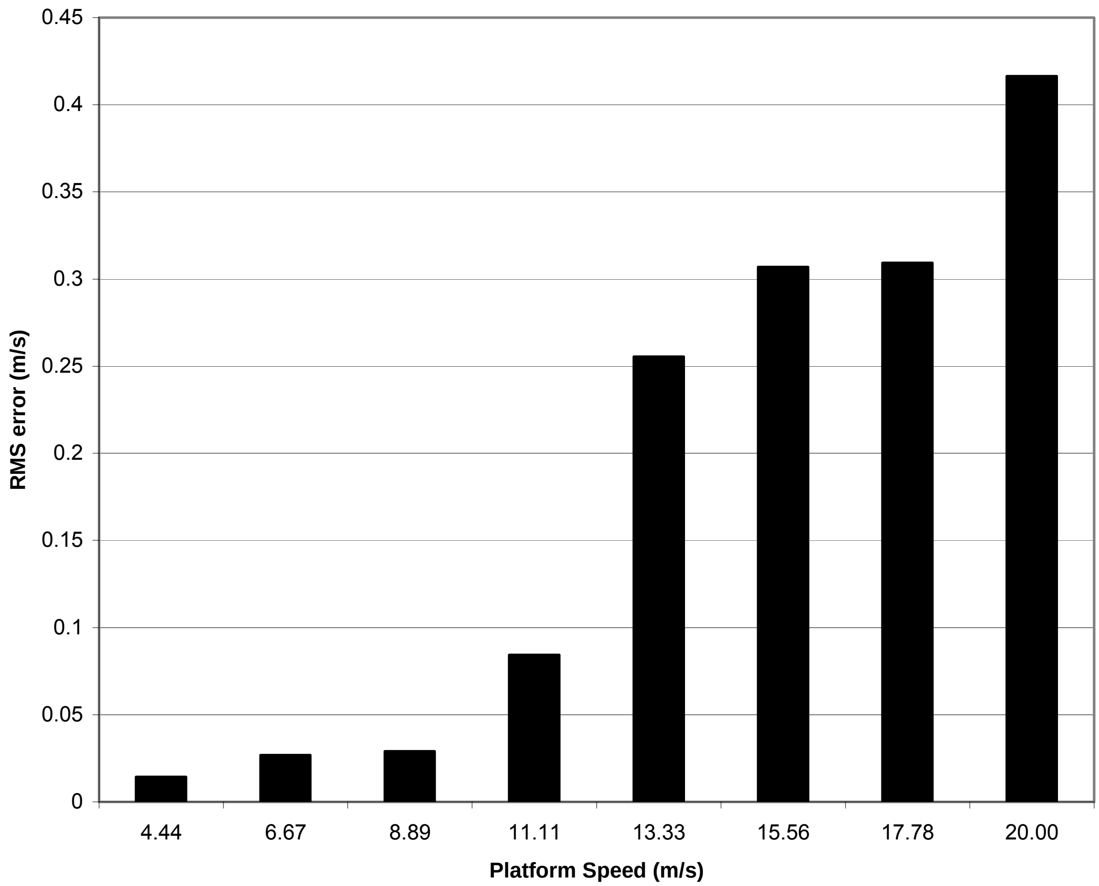


FIG. 3. Constant flow OSSE RMS error (m $s^{-1}$) as a function of platform velocity (m $s^{-1}$) for a fixed scan rate of 2.0 deg $s^{-1}$.

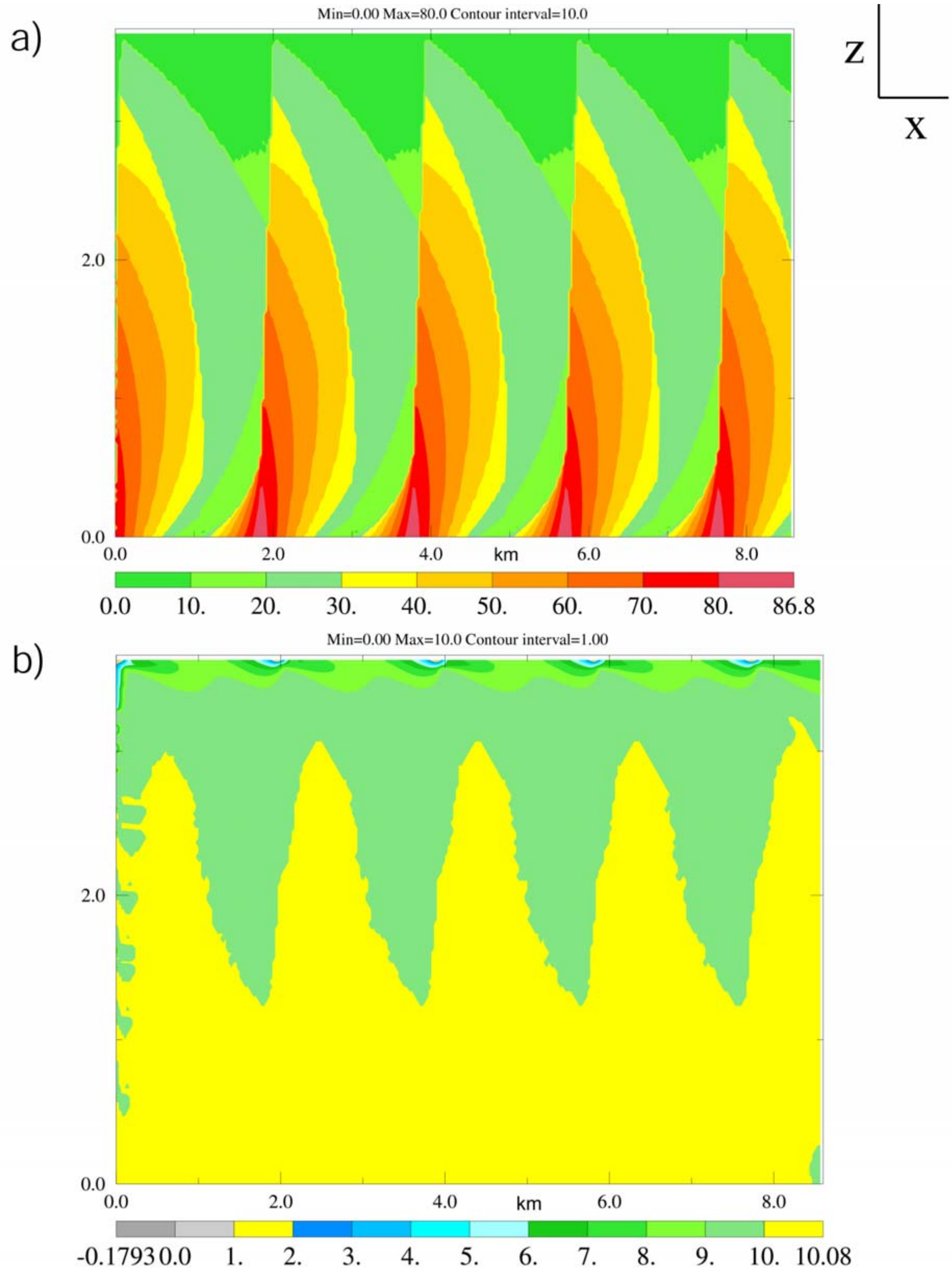


FIG. 4. a) Constant flow OSSE maximum look angle and b) analysis *u*-component wind for a scan rate of 2.0 deg $s^{-1}$ and a platform velocity of 20.0 m $s^{-1}$. The scales are indicated at the bottom of each figure. The truck is in motion from right to left. Horizontal and vertical distance scales are included.

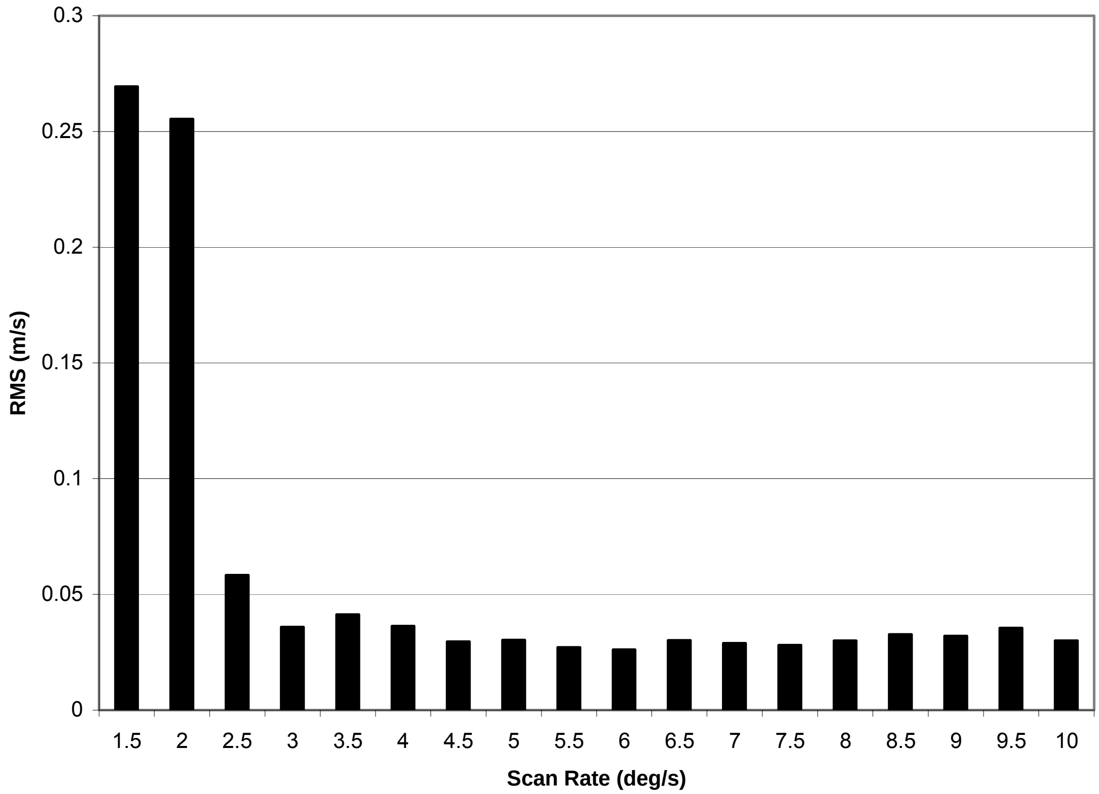


FIG. 5. Constant flow OSSE RMS error (m $s^{-1}$) as a function of scan rate (deg $s^{-1}$) for a fixed platform velocity of 13.33 m $s^{-1}$.

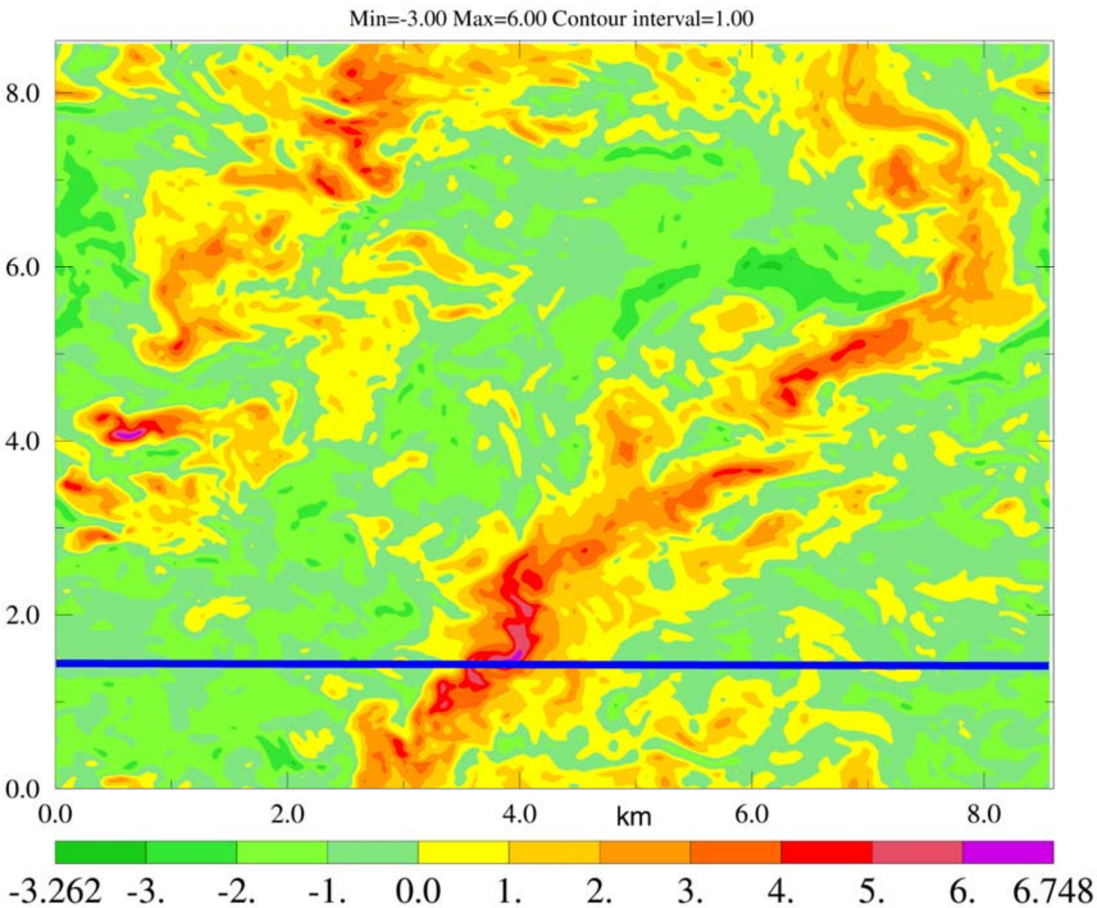


FIG. 6. LES plan image of *w* (m $s^{-1}$) at 900 m AGL. Color scale is indicated at the bottom of the image. Horizontal distance scales are indicated. The blue line represents the plane of cross section for FIG. 7a.

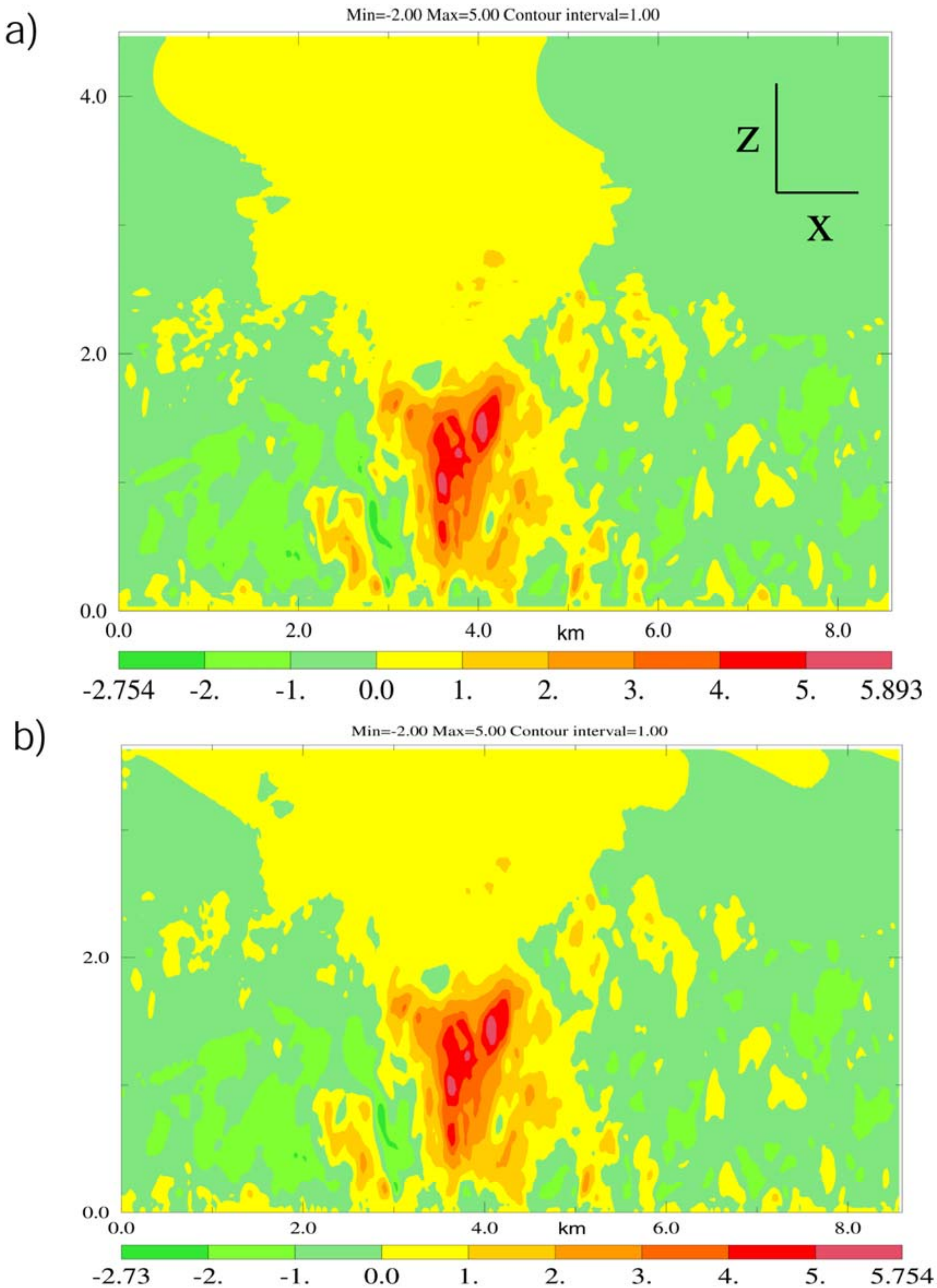


FIG. 7. a) LES cross-section of *w*-component wind ("truth") (m $s^{-1}$). b) OSSE *w*-component analysis (m $s^{-1}$) using a platform velocity of 13.33 m $s^{-1}$ and scan rate of 1.6 deg $s^{-1}$. Color scales are indicated at the bottom of each image. Horizontal and vertical distance scales are also provided.

a)

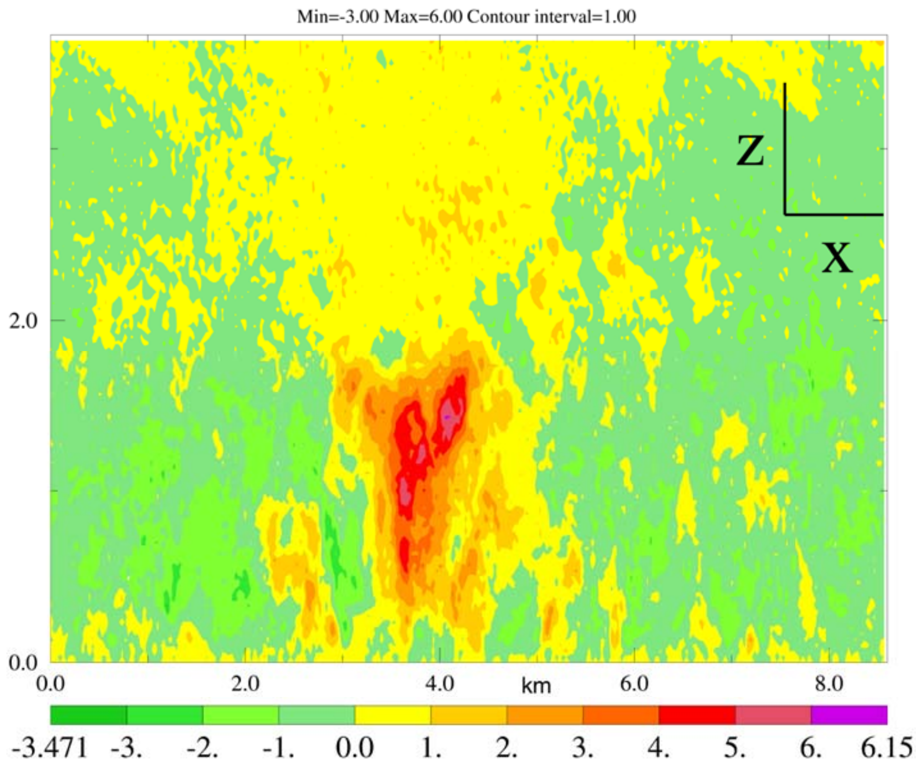


b)

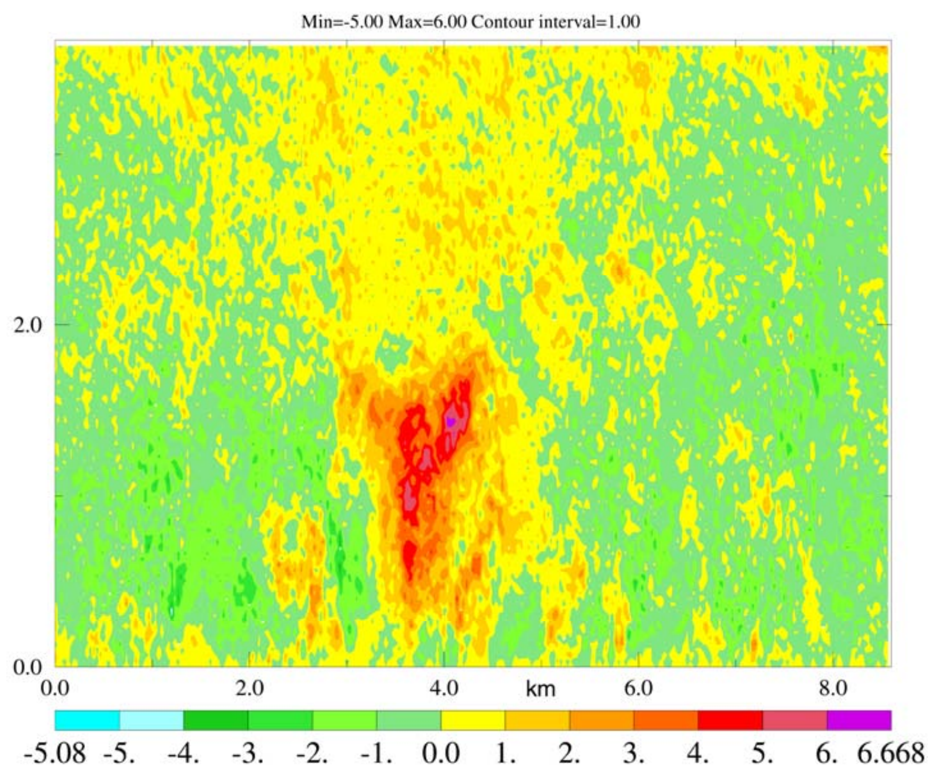


FIG. 8. LES OSSE analysis *w*-component wind (m s$^{-1}$) for a platform velocity of 13.33 m s$^{-1}$, scan rate of 1.6 deg s$^{-1}$ and an imposed Gaussian observational error of a) 1.0 m s$^{-1}$ and b) 2.0 m s$^{-1}$. The "truth" field is shown in FIG. 7a.